

# Surface-Reconstructed Icosahedral Structures for Lead Clusters

Shaun C. Hendy\*

*Applied Mathematics, Industrial Research Ltd, Lower Hutt, New Zealand*

Jonathan P. K. Doye

*University Chemistry Laboratory, Lensfield Road, Cambridge CB2 1EW, United Kingdom*

(Dated: October 27, 2018)

We describe a family of icosahedral structures for lead clusters. In general, structures in this family contain a Mackay icosahedral core with a reconstructed two-shell outer-layer. This family includes the anti-Mackay icosahedra, which have a Mackay icosahedral core but with most of the surface atoms in hexagonal close-packed positions. Using a many-body glue potential for lead, we identify two icosahedral structures in this family which have the lowest energies of any known structure in the size range from 900 to 15000 lead atoms. We show that these structures are stabilized by a feature of the many-body glue part of the interatomic potential.

## I. INTRODUCTION

The structure of an atomic cluster often differs from that of the corresponding bulk material<sup>1</sup>. In such a cluster, the number of surface atoms is comparable to the number of interior atoms, and consequently, the surface energy plays an important role in determining the overall structure. For example, regular noncrystalline structures with fivefold axes of symmetry, such as icosahedra and decahedra, are known to occur in gold and a variety of other face-centered cubic (fcc) metals<sup>1,2,3</sup>. Such structures are comprised of deformed fcc tetrahedral units where adjacent tetrahedral faces meet at a twin plane. The energy cost of twinning at the inner tetrahedral faces, and the strain energy in the deformed tetrahedra, is overcome by the resulting energetically favorable close-packed outer faces<sup>4,5</sup>.

The structure of a cluster, while not only of fundamental interest, is also a key determinant of many of its properties. However the delicate balance between surface and internal energies often produces a complex dependence of structure upon cluster size<sup>6,7</sup>. Eventually, as the size of a cluster increases, the bulk structure must win out, but at sizes below this, clusters can assume a variety of regular non-crystalline structures. For systems that can be adequately described by pair potentials, there is a relatively good understanding of how structure depends on the form of the potential<sup>8,9</sup>. However, for many systems of interest, such as metals, the interatomic interactions are more complex.

Metals exhibit a strong many-body character to their bonding, and because of this, the competition between fcc, icosahedral and decahedral structures is less well understood. In addition, many-body effects can potentially lead to the emergence of new structural forms<sup>10,11</sup>. In order to study the effect of this bonding on structure, it is often necessary to resort to empirical potentials, as *ab initio* electronic structure methods are prohibitively expensive for all but the smallest cluster sizes. For example, lead clusters have been studied using a many-body glue potential<sup>12,13</sup>. The first comprehensive computa-

tional study of lead cluster structure, by Lim, Ong and Ercolessi<sup>14</sup>, utilized this potential to compare the energetics of closed-shell fcc cuboctahedral and Mackay icosahedral structures for cluster sizes from 55 to 3871 atoms. By directly comparing the binding energies at the same numbers of atoms for each structure, they demonstrated that the fcc cuboctahedra were favored over Mackay icosahedra over this size range.

However, electron diffraction of 3-7 nm lead clusters has produced diffraction patterns that cannot be adequately fitted by fcc structural models<sup>15</sup>. In addition, recent simulations of the melting and freezing of clusters, using the same glue potential as Lim, Ong and Ercolessi<sup>14</sup>, have unexpectedly revealed that fcc structures were not the lowest in energy in this size range<sup>16</sup>. In these simulations, clusters were prepared by the quenching of liquid lead droplets. This procedure was found to produce icosahedra overwhelmingly, and these resolidified icosahedra were found to be energetically favored over fcc structures<sup>14</sup>. The resolidified icosahedra resembled anti-Mackay icosahedra<sup>17</sup> which have a Mackay icosahedral core but with most of the outer layer in hexagonal close-packed (hcp) surface sites. The improved stability of these icosahedra was evidently due to this surface reconstruction.

The purpose of this work is to examine the surface reconstruction of these resolidified icosahedra in more detail. In particular, we will show that the surface reconstruction is similar, but not identical, to that of the anti-Mackay icosahedra. These surface features lead us to identify a new family of icosahedral structures, of which the anti-Mackay icosahedron is a member. We will describe these structures in detail, and show how they can lead to lower energy structures for the lead glue potential.

## II. COMPUTATIONAL TECHNIQUES

### A. Molecular dynamics

Molecular dynamics was performed using a local version of the classical molecular dynamics code ALCMD, originally developed by Ames Laboratory. Finite temperature simulations were performed in the microcanonical ensemble (i.e. constant energy). The time step was chosen as 3.75 fs throughout. Melting and freezing simulations were carried out using the procedure detailed in Hendy and Hall<sup>16</sup>.

The inter-atomic potential used is due to Lim, Ong and Ercolessi<sup>14</sup>. This is a many-body glue-type potential, given by

$$\begin{aligned} E &= E_{\text{pair}} + E_{\text{glue}}, \\ &= \sum_{i < j} \phi(r_{ij}) + \sum_i U(n_i), \end{aligned} \quad (1)$$

where  $\phi$  is a short-range pair potential and  $U(n)$  is a many-body glue term which reflects the effects of non-local metallic bonding. The quantity  $n_i$  is a “generalized coordination number” for atom  $i$  defined as:

$$n_i = \sum_j \rho(r_{ij}) \quad (2)$$

where  $\rho$  is some short-ranged “atomic density” function. In practice, the function  $\rho(r_{ij})$  has a cut-off  $r_{\text{cut}}$ , beyond which  $\rho(r_{ij}) = 0$ , and for the potential here, a value of  $r_{\text{cut}} = 5.503\text{\AA}$  is used. This cut-off typically lies between the second and third neighbor shells. The three functions  $\phi$ ,  $\rho$  and  $U$  have been obtained by fitting to a number of known properties of lead including cohesive energy, surface energy, elastic constants, phonon frequencies, thermal expansion and melting temperature<sup>12</sup>. This potential has been used previously to model lead clusters<sup>14,16,18</sup>, temperature-dependent surface reconstructions of low-index lead surfaces<sup>19</sup> and pre-melting of low-index lead surfaces<sup>20</sup>. Recently, putative global minimum energy cluster structures were determined for this potential, for cluster sizes of up to 160 atoms<sup>11</sup>.

### B. Common neighbor analysis

Common neighbor analysis<sup>21</sup> (CNA) has been used here to analyze cluster structures<sup>7,22</sup>. CNA is a decomposition of the radial distribution function (RDF) according to the local environment of each pair. We consider that the first peak in the RDF represents “bonded” neighbors. As such, if  $r_c$  is the first minimum in the RDF, we classify any pair separated by  $r < r_c$  as a bonded pair. With this identification, any pair contributing to the RDF can be classified by a set of three indices,  $ijk$ , which provide information on the local environment of the pair. The first index,  $i$ , is the number of bonded neighbors common to

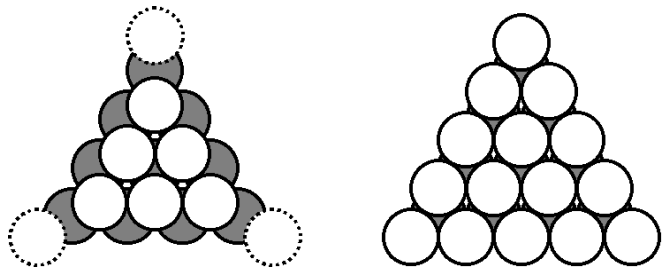


FIG. 1: The anti-Mackay surface termination (left) has surface atoms in hcp positions. The surface terminations considered here do not include the vertex atoms (indicated by the dotted lines). The Mackay surface termination (right) is shown for comparison.

both atoms. The second index,  $j$ , is the number of bonds between this set of common neighbors. The third index,  $k$ , is the number of bonds in the longest continuous chain formed by the  $j$  bonds between common neighbors.

CNA is useful here because it allows one to distinguish between local atomic arrangements, including fcc and icosahedral environments, using the type and number of  $ijk$  indices of each atom. For each atom, we can define  $n_{ijk}$  to be the number of bonds of this atom with CNA indices  $ijk$ . We can then classify the local environment of each atom using these  $n_{ijk}$  values. In Table I we have listed the classifications of CNA signatures used here to label the local environment of an atom (this classification is similar but not identical to that used by Cleveland, Luedtke and Landman<sup>22</sup>). We note that these signatures are based only on the CNA decomposition of the first peak in the RDF.

## III. ANTI-MACKAY ICOSAHEDRA

We will refer to an icosahedron with an anti-Mackay surface termination as an anti-Mackay icosahedron. With such a surface termination, atoms in the exterior shell lie in hcp positions relative to a core Mackay icosahedron, as illustrated in figure 1. Note that for the terminations we will consider here, we neglect the icosahedral vertex atoms on the surface since these are not present in the resolidified icosahedra, and tend to increase the overall energy of the cluster.

An  $n$ -shell anti-Mackay icosahedron contains a core  $(n-1)$ -shell Mackay icosahedron with  $1/2(n-3)(n-4) + 3(n-2)$  surface atoms per face (neglecting the 12 vertices). The total number of atoms in an  $n$ -shell Mackay icosahedron is

$$\text{Ico}(n) = \frac{10}{3}n^3 + 5n^2 + \frac{11}{3}n + 1, \quad (3)$$

giving the sequence 55, 147, 309, 561, 923, 1415, 2057, 2869, 3871 ... Hence, the total number of atoms in an  $n$ -shell anti-Mackay icosahedron is

$$\text{Anti}(n) = \frac{10}{3}n^3 + 5n^2 - \frac{19}{3}n - 1 \quad (4)$$

TABLE I: Description of CNA signatures used.

label	description	position	classification of pairs
A	fcc internal atom	internal	$n_{421} \geq 4$
B	fcc $\{111\}$ face atom	surface	$n_{311} \geq 3$ and $n_{322} = 0$
C	fcc $\{100\}$ face atom	surface	$n_{211} \geq 3$
D	fcc $\{111\}/\{100\}$ edge atom	surface	$n_{211} = 2$ and $n_{311} = 2$
E	internal atom at a $\{111\}$ fcc stacking fault	internal	$n_{422} \geq 5$
F	internal icosahedral atom (spine or central atom)	internal	$n_{555} \geq 2$
G	surface icosahedral apex atom	surface	$n_{555} \geq 1$
H	surface icosahedral $\{111\}/\{111\}$ edge atom	surface	$n_{311} \geq 3$ , $n_{322} \geq 1$ and $n_{322} \geq 1$
I	anti-Mackay surface $\{111\}/\{111\}$ edge atom	surface	$n_{311} = 2$ , $n_{200} = 2$ and $n_{211} \geq 1$
?	unclassified signature (possibly disordered)	internal/surface	

This gives a sequence of closed-shell anti-Mackay icosahedra with numbers of atoms as follows: 115, 267, 509, 861, 1343, 1975, 2777, 3769, 4971, 6403, 8085 ...

Thus, the  $n$ -shell anti-Mackay icosahedron contains  $10n+2$  fewer surface atoms than the  $n$ -shell Mackay icosahedron, so the packing of the surface atoms will be less dense. However, these missing atoms come from edges and vertices with low coordination  $n_i$ . Table II compares the energy of an 8-shell Mackay icosahedron and an 8-shell anti-Mackay icosahedron, broken down by CNA label. Here we can see that while the surface binding energy per atom is worse for the anti-Mackay icosahedron, the binding energy per atom for the cluster as a whole is better than the Mackay icosahedron. Thus for the potential (1), this removal of edges and vertices from the Mackay icosahedron (which can be seen to have particularly poor energetics in Table II), improves the total energy per atom.

However, despite this improvement in the binding energy of the anti-Mackay icosahedra, they are still not energetically competitive with the cuboctahedra sequences or the resolidified icosahedra, as shown in figure 2 (note that here we refer to cuboctahedra with triangular  $(111)$ -faces simply as cuboctahedra, and to cuboctahedra with hexagonal  $(111)$ -faces as truncated octahedra). Thus, while the resolidified icosahedra and the anti-Mackay icosahedra share a similar surface reconstruction, the resolidified icosahedra have other features which account for their more favorable energetics. We will discuss these features in the next section.

#### IV. RESOLIDIFIED ICOSAHEDRA

Hendy and Hall<sup>16</sup> conducted a series of resolidification trials, where lead clusters were melted and then resolidified at constant energy. Figure 3 shows the distribution of binding energies of 2057-atom clusters that emerged from a typical sequence of 25 resolidification trials (more details can be found in Hendy and Hall<sup>16</sup>). These trials typically produce icosahedron-like structures, similar to

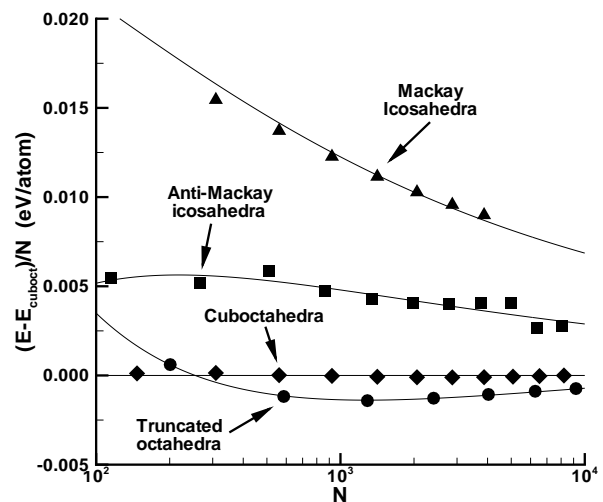


FIG. 2: Energies of clusters versus size: anti-Mackay icosahedra (solid square), cuboctahedra (solid diamond), Mackay icosahedra (solid triangle) and truncated octahedra (solid sphere). The energies are given relative to a fit to the energies of the cuboctahedra sequence:  $E_{\text{cuboct}} = -2.0293N + 1.8216N^{2/3} + 0.7134N^{1/3}$ .

that shown in figure 4, which have higher binding energies than comparably-sized fcc clusters such as cuboctahedra or truncated octahedra. In fact, the cluster shown in figure 4 had the highest binding energy produced in the trial. Hendy and Hall<sup>16</sup> noted that these icosahedron-like clusters had similar surface reconstructions to the anti-Mackay clusters.

In table II, we compare the structures of an anti-Mackay icosahedron and a resolidified icosahedron of a similar size. A crucial difference is the denser surface packing of the resolidified icosahedron. The number of atoms on the surface is comparable to that of the Mackay icosahedron (see table II), without the inclusion of energetically unfavorable edge atoms. Instead, there are a

TABLE II: Comparison of average energies of a closed-shell Mackay icosahedron, a closed-shell anti-Mackay icosahedron, a resolidified icosahedron and a  $m = 7$  surface-reconstructed icosahedron.

Signature	Cluster							
	Mackay Icosahedra		Anti-Mackay Icosahedra		Resolidified Icosahedra		$m = 7$ Icosahedra	
	N	$\langle E \rangle$ (eV/atom)	N	$\langle E \rangle$ (eV/atom)	N	$\langle E \rangle$ (eV/atom)	N	$\langle E \rangle$ (eV/atom)
A (fcc)	700	-2.0159	400	-2.0264	468	-2.0048	467	-2.0062
B (111)	420	-1.6254	200	-1.5836	173	-1.6963	185	-1.6780
C (100)	-	-	1	-1.4007	75	-1.6425	82	-1.6254
D (fcc edge)	-	-	-	-	2	-1.2624	-	-
E (hcp)	630	-2.0103	750	-2.0071	654	-2.0082	646	-2.0083
F (ico)	85	-1.9916	265	-1.9794	183	-2.0016	195	-1.9990
G (surf ico)	12	-1.0555	-	-	15	-1.7832	1	-1.7702
H (ico edge)	210	-1.4633	-	-	1	-1.9126	-	-
I (anti edge)	-	-	298	-1.5531	230	-1.6301	276	-1.6212
? surface	-	-	61	-1.3585	137	-1.5031	83	-1.6652
? interior	-	-	-	-	119	-1.9810	138	-1.9811
surface	642	-1.5617	560	-1.5425	633	-1.6251	627	-1.6181
bulk	1415	-2.0120	1415	-2.0074	1424	-2.0040	1446	-2.0038
total	2057	-1.8714	1975	-1.8755	2057	-1.8874	2073	-1.8871

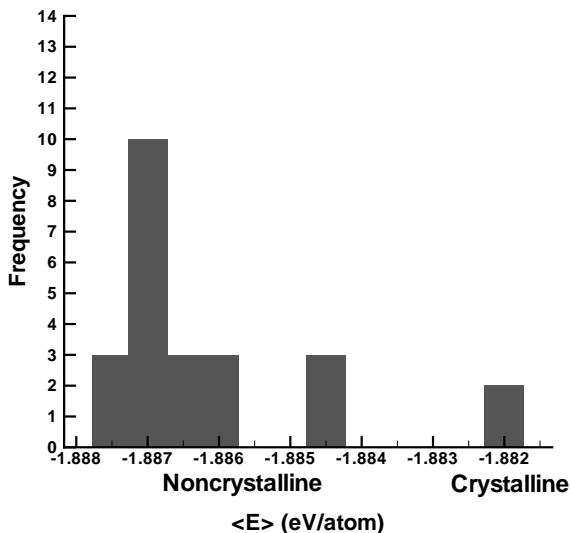


FIG. 3: Histogram showing the distribution of energies ( $\langle E \rangle$ ) for 25 resolidified 2057 atom clusters. Two resolidified clusters were identified as fcc truncated octahedra (with energies of approximately -1.8820 eV/atom) while the remaining 23 were identified as icosahedron-like (energies below -1.8840 eV/atom).

number of extra  $\{100\}$ -facets (see figure 4) distributed about the surface. Consequently, the binding energy of the surface atoms of the resolidified icosahedron is substantially larger than that in both the Mackay and anti-

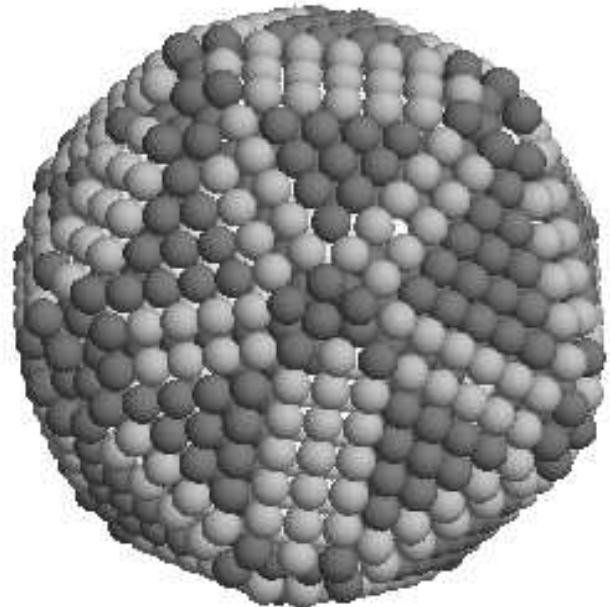


FIG. 4: A 2057-atom resolidified icosahedra. Note the anti-Mackay type surface reconstruction but also the extra  $\{100\}$ -facet. This structure had the highest binding energy of any cluster produced in the resolidification trials.

Mackay icosahedra.

A closer examination of the resolidified icosahedra reveals how they differ from anti-Mackay icosahedra. Re-

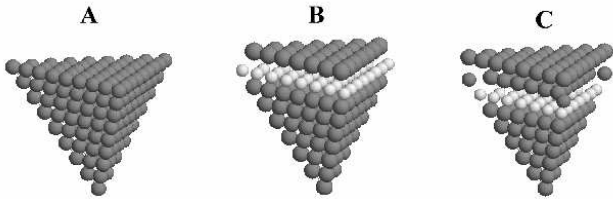


FIG. 5: Tetrahedron with a regular Mackay surface termination (A), an anti-Mackay surface termination with a stacking fault in the penultimate layer (B), and tetrahedron with a twin plane one layer lower (C).

call that a Mackay icosahedron can be constructed from twenty fcc tetrahedra. Likewise, an anti-Mackay icosahedron can be constructed from twenty tetrahedra, each of which has a surface with atoms in hcp positions, as shown in figure 5. We refer to the tetrahedra that make up a Mackay icosahedron as type A. The tetrahedra that make up an anti-Mackay icosahedron will be referred to as type B. Note that the type B tetrahedra has a stacking fault in the penultimate layer (...ABCABA) as the surface atoms lie in hcp positions. The resolidified icosahedra have been found to consist of a mixture of type B tetrahedra, and a third type of tetrahedra, which we will refer to as type C. Type C tetrahedra have a twin plane in the third shell from the surface (...ABCACB). This third type of tetrahedra is also shown in figure 5.

The arrangement of these type B and type C tetrahedra for the 2057-atom resolidified cluster from figure 4, is shown in figure 6. The extra  $\{100\}$ -facets, visible in figure 4, occur at some of the edges between type B and type C tetrahedra. Table II compares the energies of the 2057-atom resolidified icosahedron, cuboctahedron and Mackay icosahedron. It is clear that this surface reconstruction considerably lowers the surface energy of the resolidified icosahedra. Overall, the 2057-atom resolidified icosahedron has a total energy per atom that is 5 meV lower than the cuboctahedron, and 16 meV lower than the Mackay icosahedron.

Table III further decomposes the total energy of 2057-atom structures into the glue and pair potential components. The resolidified icosahedron is able to achieve a considerably lower glue energy than the two conventional structures, which more than compensates for an increase in the pair energy. We can further decompose the pair energy into two parts<sup>8</sup>:

$$E_{\text{pair}} = -n_{nn}\epsilon + E_{\text{strain}} \quad (5)$$

where  $n_{nn}$  is the number of nearest neighbors,  $\epsilon$  is the depth of the pair potential and  $E_{\text{strain}}$  is the energetic penalty for pair distances that deviate from  $r_{\text{min}}$ , the position of the minimum of the pair potential  $\phi$ . Table III shows that the increase in the pair energy of the resolidified icosahedra comes chiefly from an increase in the strain energy. Thus, the surface reconstruction of the resolidified icosahedra is able to considerably improve the

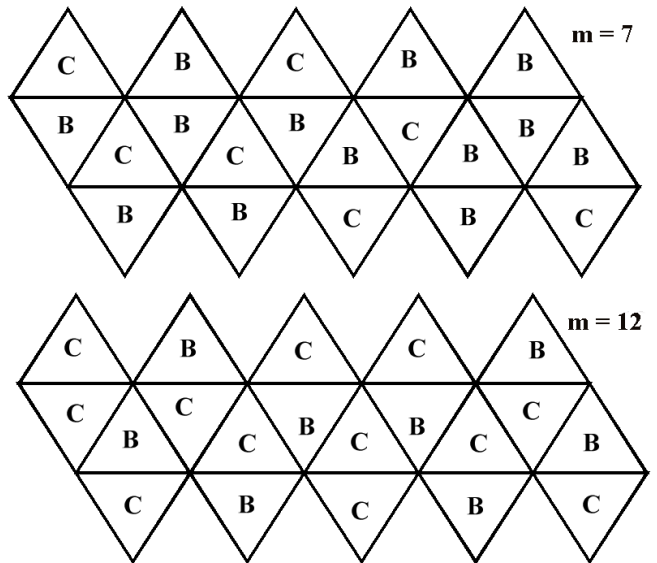


FIG. 6: This figure shows two arrangements of type-B and type-C tetrahedra considered here. The top pattern (with  $m = 7$  type-C tetrahedra) shows the arrangement of tetrahedra in the 2057-atom resolidified icosahedron shown in figure 4. The lower pattern (with  $m = 12$  type-C tetrahedra) shows the arrangement of tetrahedra in the icosahedra which appear to be stable at larger sizes.

surface energy via the glue term, incurring a smaller increase in strain energy.

We now wish to examine how the surface reconstruction improves the glue energy. It is instructive to look at the cumulative contribution to  $\langle n_i \rangle$ , from pairs with  $r_{ij} < r$  for atoms  $i$  on the surface (defined here to be atoms with  $n_i < 11$ ):

$$\langle n_i^<(r) \rangle_{\text{surf}} = \frac{1}{N_{\text{surf}}} \sum_{i \neq j, r_{ij} < r}^{\text{surf}} \rho(r_{ij}). \quad (6)$$

This quantity, and the corresponding glue energy, are compared in figure 7 for the 2057-atom cuboctahedron, Mackay icosahedron and resolidified icosahedron (note that the energy curve follows the shape of the  $\langle n_i^<(r) \rangle_{\text{surf}}$  curve as  $U$  is approximately linear away from its minimum). After the contribution to  $\langle n_i \rangle$  from the first shell ( $r_{ij} < 4.25 \text{ \AA}$  say), the Mackay icosahedron has the largest  $\langle n_i^<(r) \rangle_{\text{surf}}$  value. This is to be expected as the Mackay icosahedron has only  $\{111\}$  facets at the surface. However, for the resolidified icosahedron  $\langle n_i^<(r) \rangle_{\text{surf}}$  becomes largest beyond  $r = 4.6 \text{ \AA}$  where the contribution of the second-nearest neighbors begins to make an impact. Note that since  $n_i^<(r_{\text{cut}}) = n_i$ , it is clear from the figure that the resolidified icosahedra will have the lowest glue energy at the surface.

The relatively large contribution from next-nearest neighbors to  $n_i$ , arises due to the small difference in energy between the  $\{111\}$  and  $\{100\}$  faces for lead<sup>14</sup>. While

TABLE III: A comparison of the surface, bulk and total energies per atom of a 2057-atom cuboctahedron, a 2057-atom closed-shell anti-Mackay icosahedron and the 2057-atom resolidified icosahedron in figure 4. Also shown is the decomposition of the total energy into  $E_{\text{pair}} + E_{\text{glue}}$  (equation 1), and the strain energy  $E_{\text{strain}}$  (equation 5).

Cluster	$\langle E_{\text{bulk}} \rangle$	$\langle E_{\text{surface}} \rangle$	$\langle E \rangle$	$\langle E_{\text{glue}} \rangle$	$\langle E_{\text{pair}} \rangle$	$\langle E_{\text{strain}} \rangle$	$n_{nn}$
	(eV/atom)						
Cuboctahedron	-2.0208	-1.5901	-1.8817	-1.7368	-0.14492	0.01609	11040
Mackay Ico	-2.0141	-1.5510	-1.8714	-1.7253	-0.14614	0.01802	11256
Resolidified Ico	-2.0032	-1.6275	-1.8876	-1.7522	-0.13544	0.02634	11093

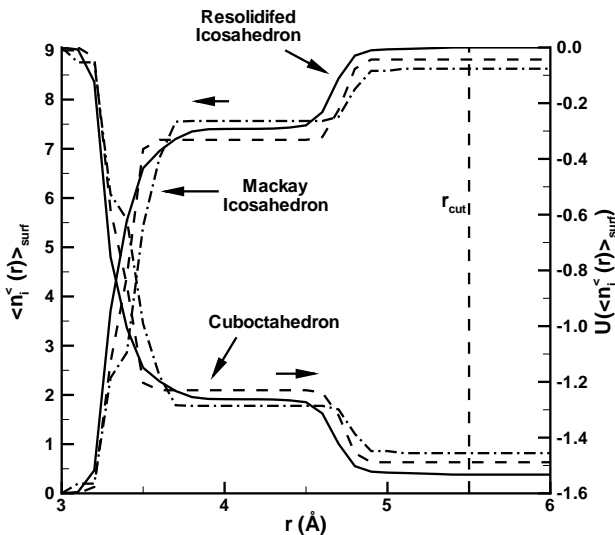


FIG. 7: A comparison of  $\langle n_i^< (r) \rangle_{\text{surf}}$  and  $U(\langle n_i^< (r) \rangle_{\text{surf}})$  for the  $m = 7$  2057-atom resolidified icosahedron (solid) in figure 6, the 2057-atom cuboctahedron (dashed) and the 2057-atom Mackay icosahedron (dash-dot). The cut-off, at which  $n_i^< (r_{\text{cut}}) = n_i$ , is indicated by the vertical dashed line.

an atom in a  $\{100\}$  face has fewer nearest-neighbors, it has more next-nearest neighbors than an atom in a  $\{111\}$  face. The glue energy reflects this small difference in energy by weighting the contributions from next-nearest neighbors more heavily than might otherwise be the case<sup>14</sup>. This would seem to be the key feature of the potential that stabilizes the novel surface reconstructions of the resolidified icosahedra.

In the next section, we will explicitly construct new icosahedra from type B and C tetrahedra. This will enable us to compare these new icosahedra to fcc structures at cluster sizes where it is currently too expensive to conduct repeated resolidification trials.

## V. NEW ICOSAHEDRA

Using the two types of tetrahedra identified in the resolidified icosahedra, we can construct  $2^{20}$  icosahedra.

However, many of the  $2^{20}$  possible icosahedra can be identified after a rotation. In the appendix, we show that there are only 17284 unique ways of constructing an icosahedron from the two types of tetrahedron.

This a large configuration space to search for the best arrangement of tetrahedra. However, a pair of clusters which are mirror images of one another will be energetically equivalent i.e. the pair will be chiral isomers. In fact, there are 1048 of the 17284 clusters which are invariant under reflections, leaving 8488 pairs of chiral isomers. This reduces the number of energetically distinct clusters to at most 9536. Further, the resolidification trials detailed in Hendy and Hall<sup>16</sup> are a way of sampling this configuration space to discover low-energy clusters.

To construct one of these new icosahedra from scratch, we begin with an  $(n - 2)$ -shell Mackay icosahedra. At faces where type-B tetrahedra are desired, add a further  $(n - 1)$ -shell Mackay icosahedral face, and at faces where type-C tetrahedra are desired, add an  $(n - 1)$ -shell anti-Mackay face. To complete the penultimate shell, Mackay icosahedral edges and vertices are added. Now to complete the outer shell, add an  $n$ -shell anti-Mackay face at faces where type-B tetrahedra are desired (the corresponding type-B tetrahedra are now layered as  $\dots ABCABA$ ), and an  $(n + 1)$ -shell anti-Mackay face where type-C tetrahedra are desired (the corresponding type-C tetrahedra are now layered as  $\dots ABC\bar{A}CB$ ).

The number of atoms in a  $n$ -shell icosahedra ( $n > 2$ ) constructed as above from  $m$  type-C tetrahedra and  $20 - m$  type-B tetrahedra is then given by:

$$\begin{aligned} \text{NewIco}(n, m) &= \text{Ico}(n - 2) \\ &+ 30n - 48 + m(n^2 - n + 1) \\ &+ (20 - m)(n^2 - 3n + 3) \end{aligned} \quad (7)$$

The cluster from figure 6, which was the best structure produced in the trials shown in figure 3, has seven type-C tetrahedra and thirteen type-B tetrahedra. With  $m = 7$ , equation 7 gives a sequence of 309, 565, 931, 1427, 2073, 2889, 3895, 5111, 8253  $\dots$  atoms in each closed-shell cluster. We note that a  $n$ -layer type-C tetrahedra contains  $2(n - 1)$  more atoms than the type-B tetrahedra and, hence a  $n$ -shell icosahedron with  $m$  type-C tetrahedra has  $2m(n - 1)$  more atoms on the surface than an  $n$ -shell anti-Mackay icosahedron (which is constructed from  $20$  type-B tetrahedra). Thus, by increasing the proportion of type-C tetrahedra, the density of surface atoms is

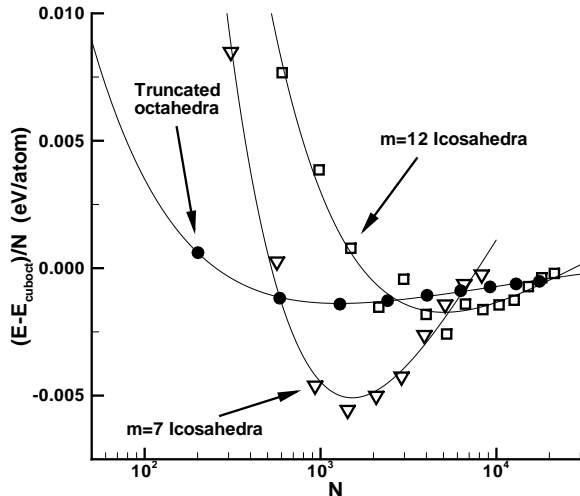


FIG. 8: Energies of clusters versus size relative to the fit to the cuboctahedra sequence:  $m = 7$  icosahedra (open gradient symbol),  $m = 12$  icosahedra (open box) and truncated octahedra (filled circle).

increased, relative to the anti-Mackay icosahedra, as seen in table II.

In table II, the energetics of a 2073-atom  $m = 7$  cluster, constructed using the design in figure 6 and then relaxed, can be compared to those of a 2057-atom resolidified icosahedron. From the CNA-classification of the atoms in these clusters, it is clear that the two clusters are very similar in structure and energetics. Although, we did not explicitly include the extra  $\{100\}$ -atoms at the outer edges in the above construction, which appear as CNA signature C in the table, these arise as the constructed cluster relaxes. An interesting feature of the structure of this cluster is that it has a chiral isomer, as the  $m = 7$  pattern 6 does not have a mirror symmetry.

Figure 8 shows the energies for a sequence of  $m = 7$  icosahedra, relative to the cuboctahedra sequence, with the first design given in figure 6. From figure 8 it appears that this type of icosahedra is the lowest energy structure for sizes from 900-5000. The largest cluster of this design that lies above the interpolated fit to the truncated octahedra sequence is the 5111-atom cluster.

We have found one other design which appears to be stable at larger sizes. This design is also shown in figure 6 and has 12 type-C tetrahedra ( $m = 12$ ). The energies of this sequence are shown relative to the cuboctahedron fit in figure 8. The first energetically favored  $m = 12$  icosahedron occurs at a size of 5211 atoms. This sequence continues to give the most energetically favored clusters we have found until a cluster size of 18097 atoms, where the truncated octahedron sequence appears to become more stable. Thus, this sequence gives the most energetically favored structures known from a size of 5211 to

15191 atoms.

## VI. DISCUSSION

We have described a new family of icosahedral structures, which include the anti-Mackay icosahedra. The family is characterized by a Mackay icosahedral core and a surface reconstruction that can extend into the two outer layers. They can be explicitly constructed from two types of fcc tetrahedra: the first type of tetrahedra has an anti-Mackay surface termination (type-B), and the second type of tetrahedra has a twin-plane fault in the third-outermost layer (type-C). The anti-Mackay icosahedra is constructed entirely from type-B tetrahedra. Structures in this family of icosahedra were shown to be the lowest energy structures known for the lead glue potential (1) for certain sizes. This study illustrates how new structural forms can arise when many-body effects are included in the interatomic potential.

Icosahedra constructed with a sufficient number of type-C tetrahedra possess a density of surface atoms comparable to that of the Mackay icosahedra, but without the low coordination atoms at the edges and vertices of a Mackay icosahedron. Such a surface reconstruction was shown to be favored by the glue-term in the interatomic potential (1) over fcc structures largely due to the effects of next-nearest neighbors. We commented that the relatively large effect that the next-nearest neighbors have on the glue term is due to the small difference in energies between the  $\{111\}$  and  $\{100\}$  faces. This next-nearest neighbor contribution is also the feature of the potential that favors fcc structures over Mackay icosahedra at all sizes, as noted by Lim, Ong and Ercolessi<sup>14</sup> in their original study of lead clusters.

While we have not exhaustively searched all possible icosahedral structures that are part of this new family, we have identified two configurations of type-B and type-C tetrahedra that show particularly favorable energetics. The first structure (which occurs in a pair of chiral isomers) has seven type-C tetrahedra and is the lowest energy structure known for the potential (1) over a size range of 900-5000 atoms. The second structure (which is symmetric under reflection) has twelve type-C tetrahedra and is the lowest energy structure known for the potential (1) over a size range of 5000-18000 atoms. Thus, above 900 atoms, fcc structures are not favoured by (1) until at least cluster sizes of 18097 atoms, where the truncated octahedra appears to be favored. This is probably a conservative lower bound on the size where large fcc structures appear as global minima of the potential (1).

These results continue to emphasize the tendency of this potential to produce non-fcc structural forms. A recent global minimization of this potential for cluster sizes of up to 160 atoms, found that these clusters do not adopt fcc structures at any size in this range<sup>11</sup>. Further, it seems likely that no globally minimum fcc structure appears in the window between that study and the results

presented here (i.e. between 160 and 900 atoms) although we have not explicitly demonstrated this here. Simulations of lead nanowires<sup>23</sup> have also shown the emergence of non-fcc structures. In all these cases, the non-fcc character is related to the small difference in energy between the {111} and {100} faces (although, disturbingly, it appears that the cut-off distance  $r$  for the glue energy also plays a role, at least for small clusters<sup>11</sup>).

We have focused here on icosahedral structures because they were produced in the melting and freezing simulations of Hendy and Hall<sup>16</sup>. While these structures were found to be lower in energy than other known structures, there is no guarantee that they are globally minimum. Indeed, simulations of freezing often produce icosahedral structures preferentially, either for thermodynamic or kinetic reasons, irrespective of whether these structures are globally optimal (see for example Chushak and Bartell<sup>24</sup>). It is possible that the novel surface reconstructions seen here may also stabilize decahedral forms, for example, which have not been seen in freezing simulations, but which may compete energetically with the icosahedral structures seen here.

## APPENDIX: N-COLORED ICOSAHEDRA

We consider painting an icosahedron using up to  $N$  colors, where each face can only be painted a single color. There are clearly  $N^{20}$  ways to paint the icosahedron, but some of these painted icosahedra will simply be rotations of other painted icosahedra.

To count the number of unique painted icosahedra we use Burnside's theorem<sup>25</sup>. Let  $X$  be the set of colorings of an icosahedron ( $|X| = N^{20}$ ) and  $G$  be the rotational symmetry group of the icosahedron ( $|G| = 60$ , consisting of the identity, 15  $180^\circ$  rotations about edges, 20  $120^\circ$  rotations about faces, and 24  $72^\circ$  rotations about vertices). Now for each  $g \in G$ , we define  $X_g = \{x \in X \mid gx = x\}$ , where  $gx$  is the new coloring obtained by rotating the coloring  $x$  via the rotation  $g$ .

Now, Burnside's theorem gives the number of colorings,  $C$ , that are unique when acted upon by the finite group  $G$ :

$$C = \frac{1}{|G|} \sum_{g \in G} |X|_g \quad (\text{A.1})$$

Thus, we can determine  $C$  by determining  $|X|_g$  for each  $g \in G$ . In fact, for each  $g \in G$ ,  $|X|_g = N^m$ , where  $m \leq 20$  is the number of orbits of faces under  $g$ . Determining the value of  $m$  for each  $g$  is straightforward, and can be done using a cardboard cut-out icosahedron (or counted on a computer).

Doing so, we arrive at the formula for  $C$  for the  $N$ -colored icosahedron:

$$C = \frac{1}{60} (N^{20} + 24N^4 + 20N^8 + 15N^{10}) \quad (\text{A.2})$$

Thus for  $N = 2$ , the number of 2-colored icosahedra is 17824.

We can also consider  $N$ -colored icosahedra under reflections as well as rotations. The size of the symmetry group is now doubled as we add a generator of reflections to the group:  $|G| = 120$ . The formula for the number of  $N$ -colored icosahedra unique under rotations and reflections is:

$$C = \frac{1}{120} (N^{20} + N^{10} + 24(N^2 + N^4) + 20(N^8 + N^4) + 15(N^{12} + N^{10})) \quad (\text{A.3})$$

Thus, if we identify mirror images, formula (A.3) applies, and hence the number of 2-colored icosahedra is 9436 ( $N = 2$ ). Of the 17824 2-colored icosahedra, 1048 are invariant under reflection symmetry, while the remaining 16776 2-colored icosahedra come in 8388 pairs of mirror images.

## ACKNOWLEDGMENTS

The authors wish to thank Peter McGavin for his help with parts of the appendix material. J. P. K. D. is grateful to the Royal Society for the award of a University Research Fellowship. S. C. H. would like to acknowledge the support of the ISAT linkages fund administered by the Royal Society of New Zealand.

\* s.hendy@irl.cri.nz

<sup>1</sup> S. Ino, J. Phys. Soc. Jpn **21**, 346 (1966).

<sup>2</sup> J. G. Allpress and J. V. Sanders, Surf. Sci. **7**, 1 (1967).

<sup>3</sup> L. D. Marks, Rep. Prog. Phys. **57**, 603 (1994).

<sup>4</sup> S. Ino, J. Phys. Soc. Jpn **27**, 941 (1969).

<sup>5</sup> L. D. Marks, Phil. Mag. A **49**, 81 (1984).

<sup>6</sup> B. Raoult, J. Farges, M. F.. De Feraudy, and G. Torchet, Philosophical Magazine B **60**, 881 (1989).

<sup>7</sup> C. L. Cleveland, U. Landman, T. G. Schaaff, M. N. Shafiqullin, P. W. Stephens, and R. L. Whetten, Physical

Review Letters **79**, 1873 (1997).

<sup>8</sup> J. P. K. Doye, D. J. Wales and R. S. Berry, J. Chem. Phys. **103**, 4234 (1995).

<sup>9</sup> J. P. K. Doye and D. J. Wales, Phys. Rev. Lett. **86**, 5719 (2001).

<sup>10</sup> J. M. Soler, M. R. Beltrán, K. Michaelian, I. L. Garzón, P. Ordejón, D. Sánchez-Portal, and E. Artacho, Physical Review B **61**, 5771 (2000).

<sup>11</sup> J. P. K. Doye and S. C. Hendy, submitted to European Physics Journal D (2002).

- <sup>12</sup> F. Ercolessi, M. Parrinello, and E. Tosatti, *Philosophical Magazine A* **58**, 213 (1988).
- <sup>13</sup> F. Ercolessi, W. Andreoni, and E. Tosatti, *Physical Review Letters* **66**, 911 (1991).
- <sup>14</sup> H. S. Lim, C. K. Ong, and F. Ercolessi, *Surface Science* **269/270**, 1109 (1992).
- <sup>15</sup> M. Hyslop, A. Wurl, S. A. Brown, B. Hall and R. Monot, *European Physics Journal D* **16**, 233-236 (2001).
- <sup>16</sup> S. C. Hendy and B. D. Hall, *Physical Review B* **64**, 085425 (2001).
- <sup>17</sup> J. P. K. Doye and D. J. Wales, *Zeit. Phys. D* **40**, 466 (1997).
- <sup>18</sup> H. S. Lim, C. K. Ong, and F. Ercolessi, *Computational Materials Science* **2**, 495 (1994).
- <sup>19</sup> C. P. Toh, C. K. Ong, and F. Ercolessi, *Physical Review B* **50**, 17507 (1994).
- <sup>20</sup> A. Landa, P. Wynblatt, H. Häkkinen, R. N. Barnett, and U. Landman, *Physical Review B* **51**, 10972 (1995).
- <sup>21</sup> A. S. Clarke and H. Jonsson, *Physical Review E* **47**, 3975 (1994).
- <sup>22</sup> C. L. Cleveland, W. D. Luedtke, and U. Landman, *Physical Review B* **60**, 5065 (1999).
- <sup>23</sup> O. Gülseren, F. Ercolessi, and E. Tosatti, *Physical Review Letters* **80**, 3775 (1998).
- <sup>24</sup> Y. Chushak, and L. S. Bartell, *European Physical Journal D* **16**, 43 (2001).
- <sup>25</sup> W. Burnside, *Theory of Groups of Finite Order* (Dover, New York, 1955), 2nd ed.